SCIENCE CHINA
Physics, Mechanics & Astronomy

• Article •

November 2014 Vol. 57 No. 11: 1–??
doi:

Jinping Underground laboratory for Nuclear Astrophysics (JUNA)

ZHANG Yu[1*] & HOU ZhanFeng[2]

[1]*Department of Physics, Liaoning Normal University, Dalian 116029, China;*
[2]*Department of Physics and the National Key Laboratory of Nuclear Physics and Technology, Peking University, Beijing 100871, China;*

Received Month date, Year; accepted Month date, Year

??????

??????

PACS number(s): ??????

Citation: ???, et al. ???. Sci China-Phys Mech Astron, 2014, 57: 1–6, doi:

1 General information

1.1 Direct measurement of cross section at Gamow energies for key reaction ^{19}F(p,α)^{16}O in AGB stars

Fluorine is one of the most important elements for astrophysics. As the unique stable Fluorine isotope, the ^{19}F abundance is very sensitive to the physical conditions within stars. Therefore, it is often used to probe the nucleosynthesis scenarios [1] of violent controversy. Most likely, fluorine can be produced: 1) during core collapse of Type II supernovae [2], 2) in Wolf-Rayet stars [3], and 3) in the convective zone triggered by a thermal pulse in asymptotic giant branch (AGB) stars [4]. Recently, fluorine overabundances by factors of 800–8000 [5] have been observed in R-Coronae-Borealis stars, providing evidence for the fluorine synthesis in such hydrogen-deficient supergiants. However, a detailed description of fluorine nucleosynthesis is still missing in despite of its crucial importance.

The major contributors to the Galactic fluorine [6] are the AGB stars. The observed fluorine overabundances cannot be explained with standard AGB models, and additional mixing is still required [7]. For example, deep mixing phenomena in AGB stars can alter the stellar outer-layer isotopic composition due to proton capture at low temperatures ($T_9 \leqslant 0.04$), and affect the transported material [8–10]. In this environment (corresponding to Gamow window [11] at $E_{c.m.}$ ~27–94 keV in the center-of-mass frame), the main fluorine destruction reaction of ^{19}F(p,α)^{16}O possibly modifies the fluorine surface abundances [1,12]. As for the hydrogen-deficient post-AGB stars, hydrogen admixture plays a key role to reverse the effect of excessive He burning and yields elemental abundances in better agreement with observations [13]. Here, the ^{19}F(p,α)^{16}O reaction might bear a great importance as it would remove both protons and fluorine nuclei from the nucleosynthesis scenario. The ^{19}F(p,α)^{16}O cross section should be determined at $E_{c.m.}$~50–300 keV for accurate modeling because of the temperature at the base of the accreted material approaching T_9~0.2 [5].

*Corresponding author (email: dlzhangyu@yahoo.com.cn)

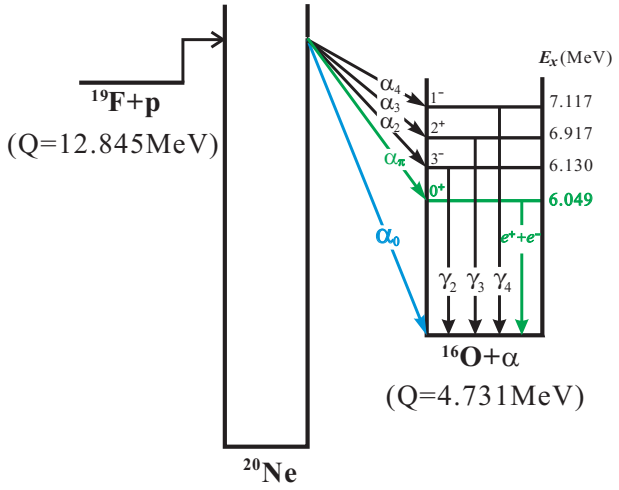

Figure 1 Reaction scheme of ^{19}F(p,α)^{16}O.

1.1.1 Available data

The reaction scheme for ^{19}F(p,α)^{16}O is shown in Fig. 1. It shows that this reaction occurs through three different types of channels: (p,α_0), (p,α_π and (p,α_γ). Where, (p,α_0) The thermonuclear reaction rates of ^{19}F(p,α)^{16}O have been evaluated in the NACRE compilation [14]. Based on a later work [15], the roles of three reaction channels are compared as shown in Fig. 2. It shows that the (p,α_0) channel dominates the total rate below ~0.1 GK; the (p,α_γ) channel dominates above ~0.15 GK; both two channels dominates over 0.1–0.15 GK. Here, contribution from the (p,α_γ) channel is negligible based on our current knowledge about this reaction.

The recommended ^{19}F(p,α_0)^{16}O astrophysical $S(E)$-factor was determined from several works [16–24] in the NACRE compilation, with the lowest energy direct data at $E_{c.m.}$=461 keV [17]. The Gamow window is only partially covered by the unpublished data of Lorentz-Wirzba [25], which were utilized [26, 27] later to evaluate the astrophysical factor in the zero and finite-range Distorted Wave Born Approximation (DWBA) approaches. These data support a strong suppression of compound ^{20}Ne decay to the ground state of ^{16}O at E_{cm}~0.14–0.6 MeV. However, these results were not included in the NACRE compilation as possible systematic errors affecting the absolute normalization might lead to an underestimate of $S(E)$ by a factor of two [14]. The astrophysical factor was then extrapolated to low energies assuming a dominant contribution of the non-resonant part [14]. This conclusion disagrees with the older measurement [17], where the existence of two resonances with J^π=1$^-$ and 0$^+$ had been reported at E_{cm}~0.4 MeV. Actually, additional resonances might be populated in ^{20}Ne [28]. A recent experiment [29] measured the ^{19}F(p,α_0)^{16}O astrophysical $S(E)$-factor by indirect means of the Trojan Horse method, and found that the largest rate difference, about 70%, occurs at temperatures relevant for post-AGB stars (~0.1 GK), exceeding the upper limit set by the previous uncertainties [14]. Such difference is clearly due to the presence of the 113 keV resonance (E_x=12.957 MeV, 2$^+$). However, the energy resolution was not enough for achieving a good separation between resonances, thus preventing an accurate estimate of the their total widths as well as the reaction rate.

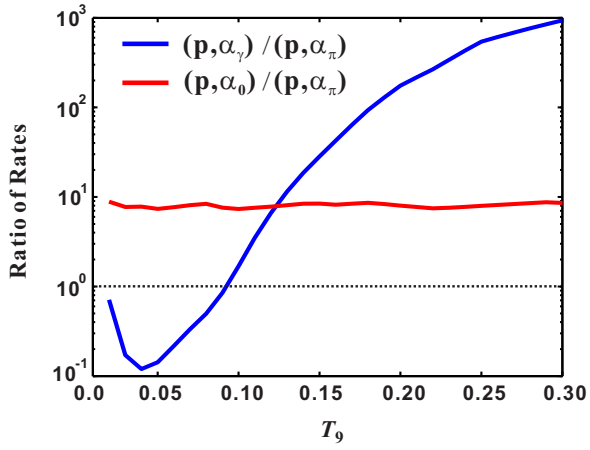

Figure 2 The role of three reaction channels contributing to the total reaction rate of ^{19}F(p,α)^{16}O.

The recommended ^{19}F(p,α_γ)^{16}O astrophysical $S(E)$-factor in the NACRE compilation has been derived from the earlier works [30–37] down to $E_{c.m.}$=957 keV. Later on, Spyrou et al. measured this channel down to ~189 keV with a 4π NaI summing spectrometer. Where, the strengths of all resonances at E_p=200–800 keV, including a new one at E_R=237 keV, have been extracted. Furthermore, the width of the important 1$^+$ resonance at E_R=11 keV was estimated, which affects the S-factor dramatically within the Gamow region owing to the inference effects with the strong 1$^+$ resonance at E_R=340 keV. Therefore, this width needs to be determined experimentally.

In a summary, there are currently no direct experimental data below $E_{c.m.}$=460 keV for the (p,α_0) channel, and below $E_{c.m.}$=190 keV for the (p,α_γ) channel. In this project, we will target on measuring the cross sections of these two reaction channels at JUNA. The experimental data for these two reaction channels are shown in Fig. 3, where the targeted regions are indicated. As a final goal, we may obtain the reliable reaction rate with the direct experimental data, and implement this new rate into the nucleosynthesis model to achieve a better understanding of the fluorine overabundances in AGB stars.

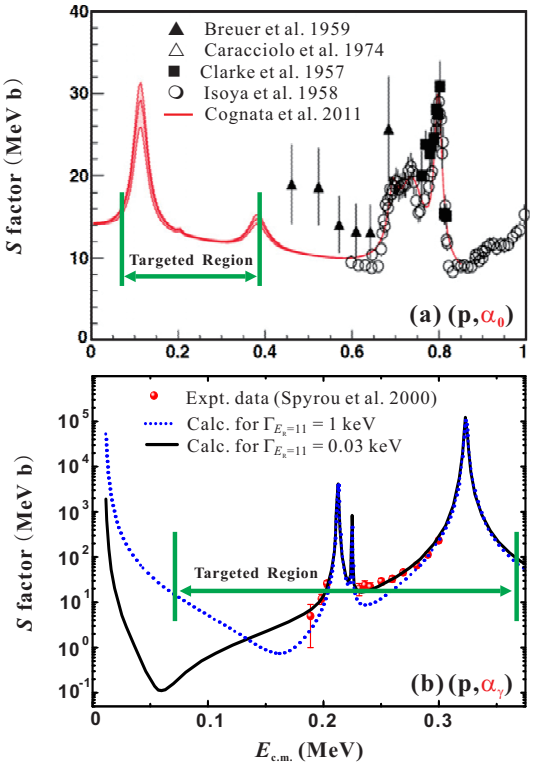

Figure 3 Available experimental data and calculations for the reaction channels of (a) (p,α_0) [14, 29], and (b) (p,α_γ) [15]. The green arrows indicate the energy regions targeted for the JUNA experiment.

1.1.2 Experimental setup

In the proposed ^{19}F$(p,\alpha)^{16}$O experiment, two reaction channels of (p,α) and (α,p) will be measured separately. The details for these two measurements will be described as below.

A 'lamp'-type Micron silicon [38] array will be constructed for the charged-particle measurement, which can cover about 4π solid angle. This universal detection array will set the base for other (p,α) and (α,p) reaction studies at JUNA. A conceptual design is shown in Fig. 4. It can not only measure the total (p,α_0) cross section but also the angular distribution. The angular distribution measured is much useful for determining the nuclear structure of the 1^+ resonance at E_R=11 keV as discussed above. In this experiment, a very thin about 4μg/cm^2 CaF_2 target will be utilized, which is evaporated on a thin backings. Thanks to the very high Q value (about 8.11 MeV) for this reaction, the average energy for the emitted α particles is about 6.7 MeV. These relatively high-energy αs can penetrate the backings and can be detected easily at the forward angle. The detectors at the forward angle do not face the Rutherford-scattered strong proton beam which is stopped in the backings. However, those detectors at the backward angle should be shielded by a thin foil, e.g., a mylar foil, to stop the scattered protons. The target backing will be connected to a cooling device to release the heat during the experiment. In addition, the classical Faraday Cup can not be used in this setup so we monitor the beam with New Parameters Current-mutual-induction Technology (NPCT) developed by the Bergoz Company in France [39].

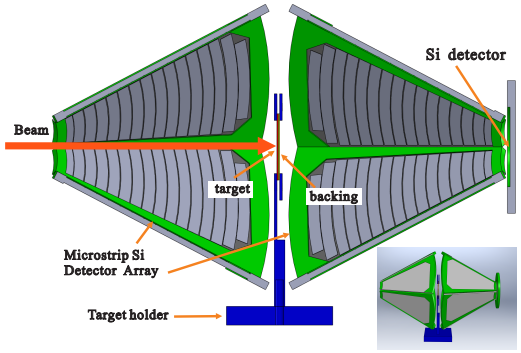

Figure 4 Conceptual silicon detector array designed for measuring the charged particles.

As for the ^{19}F$(p,\alpha_\gamma)^{16}$O channel, the energies of emitted γ rays are about 6–7 MeV, where the background mainly originates from the cosmic rays. Covered with about 2400 km marbles, such background can be greatly reduce, which makes the low-energy measurements feasible. In this project, two gamma detection arrays will be constructed for the γ-ray measurements. One is the High-Purity Germanium (HPGe) Clover array whose absolute detection efficiency is about 1% [40] for the γ rays of interest, but with excellent energy resolution; another is the 4π BGO array whose absolute efficiency is about 60% [41], but with relatively worse resolution. Here, the Clover array will be utilized in the $E_{c.m.}$>140 keV energy region, while the BGO array will be used below this energy region. With the excellent resolution of the Clover detector, the possible contaminations can be resolved and identified clearly, which makes the BGO γ-ray summing reliable at lower-energy region. A conceptual design for the Clover array is shown in Fig. 5.

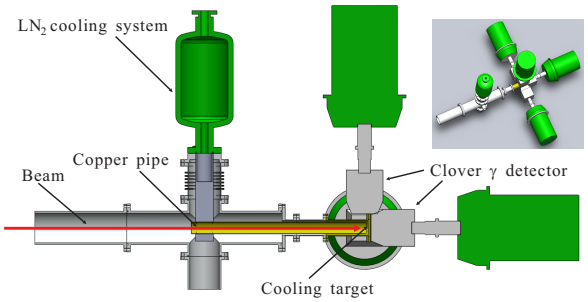

Figure 5 Conceptual Clover detector array designed for measuring the γ rays.

Table 1 α yields estimated for the (p,α_0) channel.

$E_{c.m.}$ (keV)	Cross section (b) [29]	Current (μA)	Counting rate
70	1.3×10^{-12} (pb)	100	36/week
80	9.8×10^{-12}	100	280/week
90	6.1×10^{-11}	100	240/day
100	2.4×10^{-10}	100	960/day
130	6.2×10^{-9} (nb)	10	2500/day
160	3.2×10^{-8}	1	1300/day
180	9.8×10^{-8}	1	160/hour
200	2.5×10^{-7}	1	420/hour
250	1.5×10^{-6}	1	2500/hour
350	1.6×10^{-5}	0.1	2700/hour

Table 2 γ yields estimated for the (p,α_γ) channel.

$E_{c.m.}$ (keV)	Cross section (b) [15]	Current (μA)	Counting rate	Detector
100	7.2×10^{-12} (pb)	100	20/day	BGO
110	3.1×10^{-11}	100	95/day	BGO
120	1.1×10^{-10}	100	316/day	BGO
140	1.1×10^{-9} (nb)	100	50/day	HpGe
160	7.1×10^{-9}	50	180/day	HpGe
200	2.2×10^{-7}	20	90/hour	HpGe
250	3.4×10^{-6}	5	350/hour	HpGe
300	1.0×10^{-4}	1	2100/hour	HpGe

1.1.3 Estimated yields

Yields estimated for the (p,α_0) channel:

Based on the theoretically calculated cross section in Ref. [29], the alpha yields from the (p,α_0) channel have been estimated in Table 1. In the calculations, we propose to use a 4 μg/cm^2 thickness CaF_2 target in which the energy loss of a 70-keV proton is only about 1.6 keV. The detection efficiency of the 'lamp'-type silicon array is estimated to be about 80%.

Yields estimated for the (p,α_γ) channel: Based on the theoretically calculated cross section in Ref. [15], the γ-ray yields from the (p,α_γ) channel have been estimated as listed in Table 2. This reaction becomes dominant above 0.12 GK (see Fig. 2), and the corresponding lower limit of the Gamow energy is ~100 keV. Similarly, the target thickness is also assumed to be 4 μg/cm^2 in the calculation. It can be seen from Table 2 that even at the lowest 100 keV (cross section at the order of pb), 280 counts can be expected in two weeks, with a statistical error of ~6%.

It should be noted that the JUNA 400kV accelerator can provide beam current in order of mA. This strong beam will mainly apply to those those reactions with extremely low cross section reactions (e.g., $^{12}F(\alpha,\gamma)^{16}O$) and targets with very high melting point (such as the melting point is about 3500 °C for the C target). As for the CaF_2 target, the melting point is only about 1400 °C. Here, we only assumed a 100 μA beam current. The practical highest current which the target can stand should be tested.

It can be seen from Table 1 that measurements below 90 keV energy region become increasingly difficult because of the much smaller cross section. As a conservative estimation, the highest current utilized in the present calculation is 100 μA. The experiment becomes easier with the higher current, but the target must be cooled accordingly. Based on the experience of LUNA experiments, the directly water cooled target can fully endure the supposed 100 μA current.

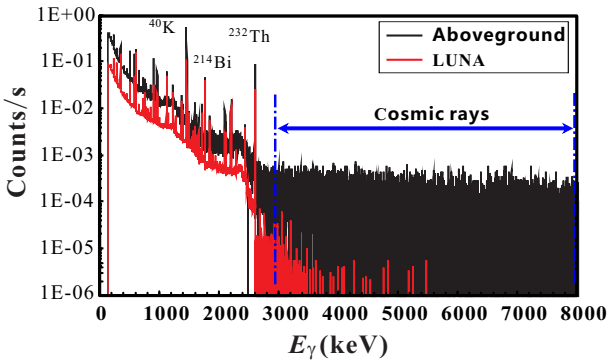

Figure 6 Comparison of γ-ray background levels at LUNA and earth surface.

Table 3 Comparison of the radioactivity background for the surrounding rocks in JUNA, LUNA and earth surface [44].

Location	^{222}Rn (Bq/kg)	^{226}Ra (Bq/kg)	^{226}Th (Bq/kg)
JUNA	20	1.8	$\leqslant 0.27$
LUNA	20–90	-	8.8
Earth surface	200–400	25	50

Table 4 Comparison of the γ-ray background levels for laboratories of JUNA, LUNA and earth surface.

Laboratory	Depth (km)	Cosmic-ray flux ($cm^{-2}s^{-1}$)	Counting rate of 3–8 MeV γ rays
JUNA	2400	2×10^{-10} [46]	2×10^{-6}/s (estimated)
LUNA	1400	3×10^{-8} [45]	2×10^{-4}/s [45]
Earth surface	~0	2×10^{-2} [47]	0.5/s [45]

1.1.4 Background estimation

Charged-particle background: In the deep underground laboratory, the environmental and material background become dominant in the charged-particle detection. All of the material used in the experiment, such as target chambers, targets and the holders, detectors and even the radiation of the shielding material can disturb the charged-particle detection [42]. For instance, the α activity of the stainless steel is one order of magnitude lower than that of the commercial aluminum material. Moreover, cosmic-ray induced γ rays, neutrons and charged particles can also affect the rare event detection. (1) In the ^{3}He(^{3}He,2p)^{4}He experiment at LUNA, the cosmic-ray induced background in the silicon detectors is as less as 3.5×10^{-4} event/s, which is about 200 times lower than that achieved aboveground [43]. The JUNA background is expected to be better than that of LUNA because of the depth.

γ-ray background: JUNA will provide an unique ultra-low background level in the world, which makes the rare-event detection possible. The 3–8 MeV γ-ray background in LUNA is about 2×10^{-4} event/s [45], ~2000 times lower than that aboveground, which is mainly caused by the cosmic rays (see Fig. 6). Owing to the depth advantage, the cosmic-ray induced background at JUNA is expected to be about 100 times lower than that in LUNA [46] (see also Table 4). Thus, the 3–8 MeV γ-ray background at JUNA is estimated to be 2×10^{-6} event/s, i.e., 0.17 event/day. By taking the beam-induced background into account, the γ background is expected to be about 0.25 event/day. Based on the above estimation, the targeted γ-ray yield at 100 keV is 13 events/day, far greater than the background level. In aboveground lab., the background level is 0.5 event/s, i.e. 4.3×10^5 events/day, which indicates only the measurements above 200 keV can be performed [15]. Consequently, JUNA can provide us an excellent condition to extend the ^{19}F(p,γ)^{16}O cross section measurement down to the Gamow energies. The background levels in LUNA, JUNA and earth-surface lab. are listed in Table 4.

(2) The neutron background in LUNA is about 3 orders of magnitude lower than that aboveground, and additionally the JUNA background is about 10 times [44] lower than that of LUNA. Therefore, the influence of neutron background on Si detectors at JUNA is about 4 orders of magnitude lower than that aboveground. (3) It was measured that the radioactivities of the surrounding rocks in JUNA is much lower than the earth surface level (see Table 3). These natural α radioactivities (together with γ radiation) will produce background in Si detectors. Furthermore, the Si detectors in the target chamber should be shielded by the *old lead* or oxygen-free copper with extremely low background. Moreover, the μ particles in cosmic ray can only deposit less than 0.5 MeV energy in the detectors, while the targeted α particles have energy loss more than 6 MeV, and therefore, the extremely low charged-particle background in JUNA makes the present measurement around 70 keV feasible.

1.1.5 Work package

This project consists of four packages: (I) Background measurement (II) Development of detector arrays (III) Test with 320kV platform at IMP (IV) Construction of experimental station.

(I) Background measurement: The underground test will be finished by the end of June in 2015 in collaboration with JUNA team. The detailed background information is the base of shielding and of selecting the material for manufacturing the chamber. And the background measured at Jinping underground lab will be utilized to make a more realistic simulation for this experiment.

(II) Development of detector arrays: Two reaction channels, i.e., ^{19}F(p,α_0)^{16}O and ^{19}F(p,α_γ)^{16}O will be measured separately in order to obtain the total cross section of the ^{19}F(p,α)^{16}O reaction studied. Therefore, two types of detec-

tors are required to be built. (1) Si charged-particle array J.J. He is the responsible person. The nuclear astrophysics group at IMP will be deeply involved in this work. (2) BGO gamma array The 4π BGO γ array will be constructed in collaboration with Prof. Zhihong Li's team (CIAE).

(III) Test with 320kV platform at IMP: In the beginning of 2015, several tests for the proposed experiment will be carried out by using the 320kV platform at IMP. The major goal of these tests is to check: (1) the stability of the thin CaF_2 target against the high current, about several tens of μA of proton; (2) the contaminants in the forward angle; (3) the chemical compositions of the target.

(IV) Construction of experimental station: Design of experimental station will be ready by the end of 2015. We plan to construct the station in 2016, which will take half a year to be accomplished.

1.1.6 Schedule

In the year of 2015, the major tasks are listed below: (I) Simulation; making a small test chamber; (II) Testing at 320kV platform; (III) Finalizing experimental plan for Jinping experiment; (IV) Purchasing Si detector and target material; designing general target chamber. In the year of 2016, the major tasks are: (I) Target making; manufacturing a general target chamber; (II) Testing at 320kV platform.

We will assemble the detector arrays at Jinping Lab and finalize their overall performance tests in 2017. The direct measurement of the proposed $^{19}F(p,\alpha)^{16}O$ experiment will be commenced in 2018. In the year of 2019, we will publish the results in the well-circulated journals and make reports in the international conferences.

This work was financially supported by the National Natural Science Foundation of China (Nos. xxx).

1 Lucatello S, et al. Fluorine and Sodium in C-rich Low-metallicity Stars. Astrophy J, 2011, 729: 40

2 Woosley S E & Haxton W C. Supernova neutrinos, neutral currents and the origin of fluorine. Nature, 1988, 334: 45–47

3 Meynet G & Arnould M. Synthesis of ^{19}F in Wolf-Rayet stars. Astron Astrophy, 2000, 355: 176–180

4 Cristallo S, et al. Evolution, Nucleosynthesis, and Yields of Low-Mass Asymptotic Giant Branch Stars at Different Metallicities. Astrophy J, 2009, 696: 797–820

5 Pandey G, Lambert D L, & Kameswara Rao N. Fluorine in R Coronae Borealis Stars. Astrophy J, 2008, 674: 1068–1077

6 Jorissen A, Smith V V, & Lambert D L. Fluorine in red giant stars: evidence for nucleosynthesis. Astron Astrophy, 1992, 261: 164–187

7 Lugaro M, et al. Reaction rate uncertainties and the production of ^{19}F in asymptotic giant branch stars. Astrophy J, 2004, 615: 934–946

8 Nollett K M, Busso M, & Wasserburg G J. Cool Bottom Processes on the Thermally Pulsing Asymptotic Giant Branch and the Isotopic Composition of Circumstellar Dust Grains. Astrophy J, 2003, 582: 1036–1058

9 Sergi M L, et al. New high accuracy measurement of the $^{17}O(p,\alpha)^{14}N$ reaction rate at astrophysical temperatures. Phys Rev C, 2010, 82: 032801R

10 Busso M, et al. On the Need for Deep-mixing in Asymptotic Giant Branch Stars of Low Mass. Astrophy J, 2010, 717: L47–L51

11 Rolfs C & Rodney W S. Cauldrons in the Cosmos. Chicago: Univ. Chicago Press, 1988

12 Abia C, et al. The First Fluorine Abundance Determinations in Extragalactic Asymptotic Giant Branch Carbon Stars. Astrophy J, 2011, 737: L8

13 Clayton G C, et al. Very Large Excesses of ^{18}O in Hydrogen-deficient Carbon and R Coronae Borealis Stars: Evidence for White Dwarf Mergers. Astrophy J, 2007, 662: 1220–1230

14 Angulo C, et al. A compilation of charged-particle induced thermonuclear reaction rates. Nucl Phys A, 1999, 656: 3–183

15 Spyrou K, et al. Cross section and resonance strength meaurement of $^{19}F(p,\alpha\gamma)^{16}O$ at E_p=200–800 keV. Eur Phys J A, 2000, 7: 79–85

16 Clarke R L & Paul E B. The angular distribution and yield of the reaction $F^{19}(p,\alpha_0)O^{16}$. Can J Phys, 1957, 35: 155–164

17 Breuer G. Messung und analyse von winkelverteilung und wirkungsquerschnitt der reaktion $F^{19}(p,\alpha_0)O^{16}$ im energiebereich 0,4 bis 0,72 MeV. Z Phys, 1959, 154: 339–351

18 Warsh K L, Temmer G M, & Blieden H R. Study of the $F^{19}(p,\alpha_0)O^{16}$ reaction with 3- to 12-MeV protons. Phys Rev, 1963, 13: 1690–1696

19 Caracciolo R, et al. The 13.645 MeV state in ^{20}Ne. Lett Nuovo Cimento, 1974, 11: 33–38

20 Cuzzocrea P, et al. Quartet states in ^{20}Ne. Lett Nuovo Cimento, 1980, 28: 515–522

21 Isoya A, Goto K, & Momota T. The angular distribution of α-particles from the reaction $^{19}F(p\alpha)^{16}O*(\pi)^{16}O$. Jour Phys Soc Japan, 1956, 11: 899–906

22 Isoya A, Ohmura H, & Momota T. The Angular Distributions of the Long-Range Alpha-Particles from the Reaction $F^{19}(p,\alpha_0)O^{16}$. Nucl Phys, 1958, 7: 116–125

23 Isoya A, Analysis of the Yield Curves and the Angular Distributions of the Reactions $F^{19}(p,\alpha_0)O^{16}$ and $F^{19}(p,\alpha_\pi)O^{16*}$. Nucl Phys, 1958, 7: 126–145

24 Morita S, et al. On the Reaction $F^{19}(p,\alpha)O^{16}$ in the Range of Bombarding Energy from 2.2- to 3.4-MeV. J Phys Soc Japan, 1966, 21: 2435–2438

25 Lorentz-Wirzba H. PhD thesis, Univ. Müster, 1978

26 Herndl H, et al. Direct reaction analysis of $^{19}F(p,\alpha)^{16}O$ below the Coulomb barrier. Phys Rev C, 1991, 44: R952–R955

27 Yamashita Y & Kudo Y. Finite-Range DWBA Analysis of (p,α) Reaction below the Coulomb Barrier. Prog Theor Phys, 1993, 90: 1303

28 Tilley D R, et al. Energy levels of light nuclei, A=20. Nucl Phys A, 1998, 636: 249–364

29 Cognata M La, et al. The fluorine destruction in stars: first experimental study of the $^{19}F(p,\alpha)^{16}O$ reaction at astrophysical energies. Astrophy J Lett, 2011, 739: L54

30 Bonner T W & Evans J E. Resonances in the Disintegration of Fluorine and Lithium by Protons. Phys Rev, 1948, 73: 666–674

31 Chao C Y, et al. Low Energy Alpha-Particles from Fluorine Bombarded by Protons. Phys Rev, 1950, 79: 108–116

32 Ask L. Angular Distributions of Alpha Particles from the Nuclear Reaction $F^{19}(p,\alpha\gamma)O^{16}$. Ark Phys, 1965, 29: 196

33 Becker H W, et al. Resonance Strengths of Some Light Nuclei. Z Phy A, 1982, 305: 319–323

34 Grambole D, et al. Fluorine determination in the near surface region of solids using the $^{19}F(p,p'\gamma)^{19}F$ resonance reaction. J Radioanal Nucl Chem, 1984, 83: 107–115

35 Croft S. The absolute yield, angular distribution and resonance widths of the 6.13, 6.92 and 7.12 MeV photons from the 340.5 keV resonance

of the ^{19}F(p,$\alpha\gamma$)^{16}O reaction. Nucl Instrum Methods A, 1991, 307: 353–358

36 Zahnow D, et al. The $S(E)$ factor of ^{7}Li(p,γ)^{8}Be and consequences for $S(E)$ extrapolation in ^{7}Be(p,γ_0)^{8}B. Z Phy A, 1995, 351: 229–236

37 Spyrou K, et al. Cross section and resonance strengths of the ^{19}F(p,$\alpha\gamma$)^{16}O reaction in the energy range E_p=0.8–3.6 MeV. Z Phy A, 1997, 357: 283–289

38 Micron Semiconductor Ltd., UK. http://www.micronsemiconductor.co.uk/.

39 Bergoz Instrumentation, France. http://www.bergoz.com/.

40 Chen S Z, et al. A new experimental setup established for low-energy nuclear astrophysics studies. Nucl Instr Meth A, 2014, 735: 466–470

41 Bemmerer D, et al. Feasibility of low-energy radiative-capture experiments at the LUNA underground accelerator facility. Eur Phys J A, 2005, 24: 313–319

42 Iliadis C. Nuclear Physics of Star. New York: Wiley-VCH, 2007

43 Greife U, et al., Laboratory of Underground Nuclear Astrophysics (LUNA). Nucl Instr Meth A, 1994, 350: 327–337

44 Seminar on underground laboratory and cutting-edge research of astrophysisc, Xichang, China, 20–22th Aug., 2013

45 Imbriani G, Int Workshop on Nucl Phys 28th Course, Italy, 16-24th Sep., 2006

46 Wu Y C, et al., Measurement of cosmic ray flux in the China JinPing underground laboratory. Chin Phys C, 2013, 37: 086001

47 Heusser G, Cosmic ray-induced background in Ge-spectrometry. Nucl Instr Meth B, 1993, 83: 223-228